



Oxidation and diffusion processes during annealing of TiSi(V)N films



F. Fernandes ^{a,*}, J. Morgiel ^b, T. Polcar ^{c,d}, A. Cavaleiro ^a

^a SEG-CEMUC – Department of Mechanical Engineering, University of Coimbra, Rua Luís Reis Santos, 3030-788 Coimbra, Portugal

^b Institute of Metallurgy and Materials Science of Polish Academy of Sciences, Krakow, Poland

^c National Centre for Advanced Tribology (nCATS), School of Engineering Sciences, University of Southampton, Highfield, Southampton SO17 1BJ, UK

^d Department of Control Engineering Czech Technical University in Prague Technicka 2, Prague 6 166 27, Czech Republic

ARTICLE INFO

Article history:

Received 22 December 2014

Revised 18 May 2015

Accepted in revised form 19 May 2015

Available online 22 May 2015

Keywords:

TiSiVN system

Structural evolution

Oxidation

Oxide scale

Diffusion processes

ABSTRACT

The degradation of self-lubricant hard coatings applied in tools for high-speed cutting or dry drilling operations occurs by a combination of wear, oxidation and diffusion. The aim of this investigation was to study the effect of V additions on the diffusion processes and on the oxide scale formation during annealing of TiSiVN coatings. Relation of these results with those achieved for a reference Ti_{0.80}Si_{0.15}N coating with similar Si content is also presented. The structure evolution of the Ti_{0.65}Si_{0.11}V_{0.15}N film was assessed by an in-situ hot-XRD device. A dual layer oxide was formed in the case of Ti_{0.80}Si_{0.15}N coating with a protective Si–O layer at an oxide/coating interface; however, in zones of film defects a complex oxide structure was developed. V additions increased the oxidation rate of the coatings as a result of the V ions diffusion throughout the oxide scale, which inhibited the formation of a continuous protective silicon oxide layer.

© 2015 Elsevier B.V. All rights reserved.

1. Introduction

The reduction of the wear and friction coefficient of machining tools during in-service conditions remains an important challenge today in order to increase their life-time and performance. Traditionally, oils and other liquid lubricants have been used to reduce the friction between the cutting tool and piece primarily by shearing the oil molecules across the solid–liquid–solid interface. However, most of the liquid lubricants volatilize at high temperature, which leads to the dry sliding and consequent failure of the cutting tools resulting in the increasing machine down times, higher process instability, poor product quality and higher costs [1]. To face these problems, a wide range of solid lubricant coatings, such as WC/C, MoS₂, diamond-like carbon (DLC), h-BN as well as their combinations in nanocrystalline or multilayer structures, have been developed in the last decades and successfully applied in order to improve the tribological behavior under dry machining conditions [2–5]. However, considerable degradation of the tribological effectiveness of these coatings at elevated temperature has been reported due to their low resistance to oxidation. To overcome this shortcoming, a new concept of high temperature lubrication has been proposed. Solid lubricant coatings have been developed by combining the intrinsic properties of some binary or ternary films (TiN, CrN, CrAlN, TiAlN, YSZ, etc.), which are very hard and resistant to oxidation, with specific elements (metals), which diffuse to the surface and form a low friction tribolayer (as a metal layer, e.g. Ag, Cu, Au, Pb and In, or a low-friction

oxide, e.g. V₂O₅, Ag₂Mo₂O₇) [6–9]. Among these elements, particular attention has been given to the vanadium-containing coatings (Magnéli phases V_nO_{2n-1}), which showed interesting tribological properties in the temperature range 500–700 °C [2,10–15]. Dissimilar series of V-based hard coatings have been developed, such as ternary CrVN [16], (V,Ti)N [17], multilayer AlN/VN [18] and quaternary single layered or multilayered AlCrVN [19,20] and TiAlVN [12,21–23]. Independent of the configuration, the friction was decreased and the wear resistance improved; however, the oxidation resistance was degraded. For example, for ternary AlCrN and TiAlN coatings the onset point of oxidation decreased to 600 °C with V incorporation [12,24,25]. In the case of the TiAlN/VN films, signals of lubricious V₂O₅ were detected as soon as the oxidation started (600 °C), while at high temperatures only AlVO₄ and TiO₂ were identified [12]. For AlCrVN coatings, AlVO₄, (Al, Cr, V)₂O₃ as well as V₂O₅ oxides were observed for an annealing temperature of 700 °C [25]. In these studies, the lower onset point of oxidation displayed by the V-containing coatings in relation to the host ones was explained by the reactions occurring between protective oxides and vanadium (such as formation of Al–V–O phases). Lower oxidation resistance of coatings due to V incorporation is not considered as a drawback from the tribological point of view, since the V₂O₅ oxide formed at the surface is known to reduce the friction and wear rate of coatings. Thus, as the oxidation behavior strongly affects the performance of the coatings, some studies were conducted with the aim of understanding the diffusion processes occurring during coatings annealing. Zhou et al. [24] and Franz et al. [25] studied TiAlN/VN and AlCrVN films, respectively. Zhou et al. [24] reported that a duplex oxide structure was formed during annealing of TiAlN/VN coatings for temperatures higher than 600 °C: an inner layer

* Corresponding author.

E-mail address: filipe.fernandes@dem.uc.pt (F. Fernandes).

comprised a porous region of Ti rich and V rich nanocrystallites, while several phases were observed in the outer region, including V_2O_5 , TiO_2 and $AlVO_4$. V_2O_5 phase was dominant in the outer surface at temperatures higher than 638 °C. The outward diffusion of V depended on the species presented: in the inner layer, V was presented as V^{3+} and V^{4+} , while V^{5+} was dominant in the outer layer. The porous inner layer was attributed to V ions diffusion to the surface to form V_2O_5 . Franz et al. [25] also observed the formation of two different oxide layers during annealing of AlCrVN coatings. While vanadium diffusion led to a V-depleted inner oxide (mixed or nanocrystalline $(Al,Cr,V)_2O_3$), the outer oxide mainly contained V_2O_5 and small amounts of $AlVO_4$. Despite of these investigations, very little knowledge is still available for the static oxidation of V rich coatings.

Recently we have reported the effect of V incorporation on the structure, mechanical properties, oxidation resistance and tribological behavior (at room temperature) of TiSiN films, deposited by DC reactive magnetron sputtering [26,27]. TiSiN system exhibits similar level of oxidation resistance than AlCrN and TiAlN films [28,29] (the only ternary films where the effect of V additions was studied); moreover, it can be deposited with much higher hardness depending on the structure and Si content. Lubricious vanadium oxides have been successfully detected on the oxidized surface and on the worn surface of these films, which decreased the wear rate and friction coefficient of coatings. However, as in the similar coating systems, a drop on the oxidation resistance of coatings was observed. In our specific case, the reaction of V with the protective oxide (Si–O) was not detected and therefore the decrease of the oxidation resistance could not be attributed to such reactions. Present work provides a comprehensive understanding of the oxidation mechanism/diffusion processes occurring during TiSiVN film annealing. The effect of vanadium was studied in comparison to the diffusion processes occurring during annealing of a $Ti_{0.80}Si_{0.15}N$ films, which were used as a reference. In addition, isothermal oxidation kinetics curves are included to provide a baseline.

2. Experimental procedure

TiSiN and TiSiVN coatings (labeled as $Ti_{0.80}Si_{0.15}N$ and $Ti_{0.65}Si_{0.11}V_{0.15}N$, respectively), with approximately the same silicon content and about 2.5 μm of total thickness, were deposited on alumina and FeCrAl alloy substrates in a d.c. reactive magnetron sputtering machine equipped with two rectangular, Ti (99.9%) and $TiSi_2$ (99.9%), magnetron cathodes working in unbalanced mode. V incorporation was achieved by inserting 8 pellets of vanadium into the erosion zone of Ti target. In both cases Ti–V (0.24 μm) and Ti–VN (0.45 μm) adhesion layers were deposited as bonding layers improving coating to substrate adhesion.

The depositions were performed with a negative substrate bias of 50 V. In both depositions, the total working gas pressure was kept constant at 0.3 Pa, using approximately 30 sccm of Ar and 17 sccm of N_2 , and the deposition temperature was lower than 300 °C. These coatings were already characterized in our previous works [26,27]. A summary of the deposition conditions and the main properties of the coatings are listed in Table 1. Temperature effect on the structure of the V rich coating was characterized in open air in-situ by hot-XRD device in the range of 500 °C to 750 °C, using a grazing incidence angle of 2° and Co K α radiation (1.789010 Å). This range of temperature was selected based on the thermogravimetric oxidation curves of films performed at a constant linear-temperature ramp (RT (room temperature) to 1200 °C at 20 °C/min) shown in Ref. [26]. Between each selected temperature a step of 10 min holding time was allowed for thermal stabilization and 30 min time acquisition was used. Oxidation of films was assessed by thermogravimetric analysis (TGA) using industrial air (99.99% purity). $Ti_{0.65}Si_{0.11}V_{0.15}N$ and $Ti_{0.80}Si_{0.15}N$ films were isothermally tested at 600 °C during 30 min and 900 °C during 1 h, respectively. These temperatures represent main oxidation events observed in the previous thermal gravimetric oxidation curves performed at constant linear-temperature ramp [26]. After annealing, the cross section thin foils of oxidized films was prepared by a focused ion beam (FIB) and analyzed by transmission electron microscope (TEM) equipped with an energy-dispersive x-ray (EDS) spectroscopy system. Bright field scan transmission electron microscopy STEM/EDX maps and elemental profiles along the cross section of the oxidized coatings were acquired to characterize the distribution of the main elements in the films ($Ti_{0.80}Si_{0.15}N$ and $Ti_{0.65}Si_{0.11}V_{0.15}N$) and in the oxide scales.

3. Results and discussion

3.1. Characterization of the as-deposited and oxidized coatings

Firstly we will summarize the main characteristics and the oxidation resistance of $Ti_{0.80}Si_{0.15}N$ and $Ti_{0.65}Si_{0.11}V_{0.15}N$ coatings. The investigated coatings with chemical composition of $Ti_{0.80}Si_{0.15}N$ and $Ti_{0.65}Si_{0.11}V_{0.15}N$, showed a typical columnar morphology and fcc NaCl-type structure assigned to crystalline TiN with Si and V in solid solution [26]. V additions to the TiSiN coating significantly improved their mechanical and tribological properties; however, their oxidation resistance was lowered. The improvement of the tribological properties was related to V–O formation in the sliding contact, which acted as a lubricious tribo-film decreasing the friction and protecting the coating from wear [27]. Fig. 1 shows the weight gain during isothermal oxidation at three selected temperatures. Note that $Ti_{0.80}Si_{0.15}N$ film was tested at higher

Table 1
Designation, deposition conditions and main properties of the $Ti_{0.80}Si_{0.15}N$ and $Ti_{0.65}Si_{0.11}V_{0.15}N$ coatings.

Sample	TiSiN					TiSiVN				
	$Ti_{0.80}Si_{0.15}N$					$Ti_{0.65}Si_{0.11}V_{0.15}N$				
Sample designation	$Ti_{0.80}Si_{0.15}N$					$Ti_{0.65}Si_{0.11}V_{0.15}N$				
Base pressure (Pa)	8.7×10^{-4}									
Working pressure (Pa)	0.3 Pa									
Target power density (W/cm ²)	Ti		$TiSi_2$			Ti		$TiSi_2$		
	6		1.5			6		1.5		
Substrate temperature (°C)	<300 °C									
Ar and N ₂ gas flow (sccm)	35 and 17									
Coatings thickness (nm)	2.5 μm									
Chemical composition	Ti	Si	V	O	N	Ti	Si	V	O	N
	41.3 ± 0.3	6.68 ± 0.03	–	0.55 ± 0.06	51.5 ± 0.2	33.6 ± 0.3	5.64 ± 0.05	7.6 ± 0.2	1.42 ± 0.13	51.71 ± 0.14
Lattice parameter (nm)	0.422					0.421				
Grain size (nm)	24					20				
Hardness (Gpa)	27 ± 2					28 ± 2				
Young's Modulus (GPa)	307 ± 10					328 ± 7				
Residual stresses (GPa)	3.4					4.1				
Onset point of oxidation	900 °C					500 °C				
Friction coefficient (room temperature) against Al_2O_3	1.07					0.51				

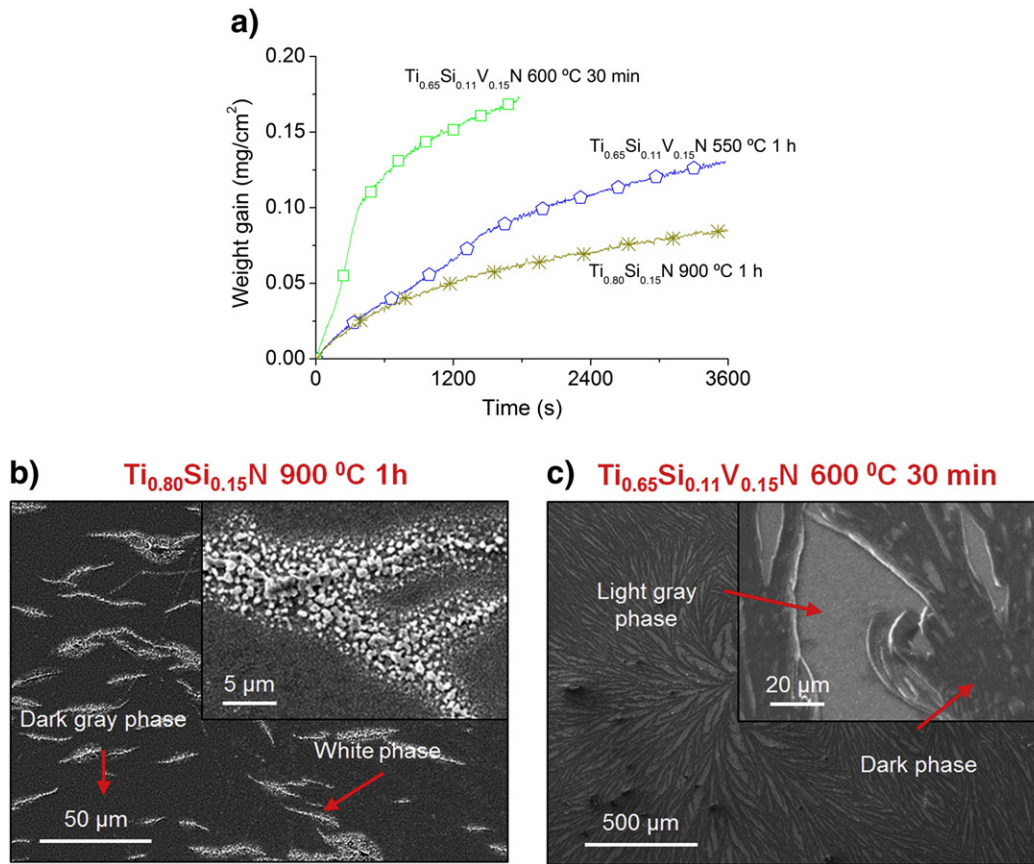


Fig. 1. a) Isothermal oxidation curves of $\text{Ti}_{0.65}\text{Si}_{0.11}\text{V}_{0.15}\text{N}$ coating tested at 600 °C during 30 min and 550 °C during 1 h and $\text{Ti}_{0.80}\text{Si}_{0.15}\text{N}$ coating tested at 900 °C during 1 h, b–c) typical surface morphologies of $\text{Ti}_{0.80}\text{Si}_{0.15}\text{N}$ and $\text{Ti}_{0.65}\text{Si}_{0.11}\text{V}_{0.15}\text{N}$ coatings annealed at 900 °C during 1 h and 600 °C during 30 min, respectively.

temperature than V rich coating since no signals of oxidation were detected at lower temperature. On the other hand, the oxidation resistance of the V rich coating could not be studied at 900 °C due to melting of V_2O_5 (~685 °C) [7,13,24] and consequent degradation of the film [26]. $\text{Ti}_{0.80}\text{Si}_{0.15}\text{N}$ displayed a typical parabolic oxidation weight gain as a function of time, which indicates the presence of protective oxide scales. The isothermal curves of $\text{Ti}_{0.65}\text{Si}_{0.11}\text{V}_{0.15}\text{N}$ films tested at 550 °C and

600 °C showed two steps: they started with a linear increase in mass gain and then followed with a parabolic evolution. The surface morphologies of the oxidized coatings are shown in Fig. 1b–c) for coatings $\text{Ti}_{0.80}\text{Si}_{0.15}\text{N}$ tested at 900 °C and $\text{Ti}_{0.65}\text{Si}_{0.11}\text{V}_{0.15}\text{N}$ oxidized at 600 °C, respectively. The detailed description of the surface oxide constitution, based on XRD diffraction, Raman spectroscopy and SEM-EDS analyses, can be found in our previous study [26]. Here we will briefly summarize

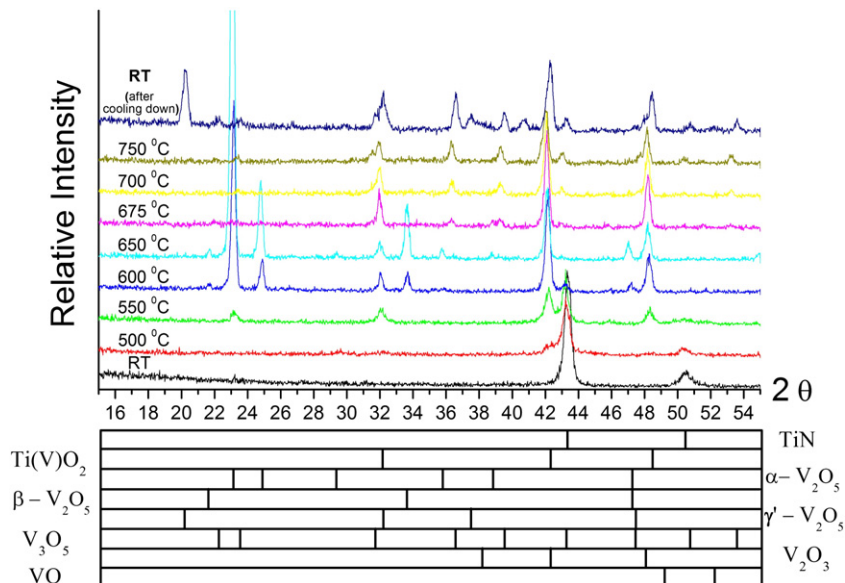


Fig. 2. XRD spectra of $\text{Ti}_{0.65}\text{Si}_{0.11}\text{V}_{0.15}\text{N}$ film at different temperatures (upper) and position of main peaks of corresponding phases (lower).

these results to support the investigation aimed at diffusion process. Annealed $\text{Ti}_{0.80}\text{Si}_{0.15}\text{N}$ film (see Fig. 1b)) exhibited two different surface features: white and dark gray islands evenly distributed on the surface. Raman analyses revealed that white phase was rutile (TiO_2), while dark gray phase was a mixture of rutile and anatase. However, only rutile peaks were detected by XRD diffraction suggesting very limited amount of anatase in the dark gray islands. Furthermore, strong signals of Si were detected on dark zone by EDS. However, the signals of silicon oxide were neither detected by XRD nor by Raman spectroscopy indicating amorphous character, which corroborates previous reports [30, 31]. Silicon oxide was positioned below Ti–O rich layer. Different morphology and oxide phases were detected on the oxidized surface of $\text{Ti}_{0.65}\text{Si}_{0.11}\text{V}_{0.15}\text{N}$ coating. At 600 °C, the film displayed a floret-like structure formed by light and dark gray phases. XRD diffraction showed the presence of $\alpha\text{-V}_2\text{O}_5$ and $\text{Ti}(\text{V})\text{O}_2$ oxides. Although EDS analysis revealed similar spectra for both phases, the much less intensity of the V peak on the light gray phase, and its conjugation with Raman analysis allowed identifying dark and light gray phases as $\alpha\text{-V}_2\text{O}_5$ and $\text{Ti}(\text{V})\text{O}_2$ oxides, respectively. Similar to $\text{Ti}_{0.80}\text{Si}_{0.15}\text{N}$ coating, signals from Si–O were neither detected by XRD nor by Raman spectroscopy. However, according

to the EDS analyses this oxide should coexist with the $\text{Ti}(\text{V})\text{O}_2$ phase as strong signals of Si coming from the sub-surface layer (light phase in Fig. 1c)). Similar phases were detected at 550 °C by XRD; however, only small dark gray areas were observed at the surface.

3.2. Phase evolution during annealing of $\text{Ti}_{0.65}\text{Si}_{0.11}\text{V}_{0.15}\text{N}$ (in situ) and growing mechanism of the V_2O_5 phase

Fig. 2 plots the high temperature in-situ XRD spectra evolution for $\text{Ti}_{0.65}\text{Si}_{0.11}\text{V}_{0.15}\text{N}$ coating together with as deposited and cooled state. The first signs of oxides were detected at 500 °C and identified as rutile type phase with V in solid solution, the $\text{Ti}(\text{V})\text{O}_2$ (ICDD card 77-0332). Further increase in temperature to 550 °C led to an increase of the $\text{Ti}(\text{V})\text{O}_2$ peaks intensity and the appearance of a new phase: the $\alpha\text{-V}_2\text{O}_5$ (ICDD card 41-1426) oxide with orthorhombic symmetry (peak at 23.6°). At 600 °C a strong increase in intensity of the $\alpha\text{-V}_2\text{O}_5$ oxide peaks with a strong preferred orientation following the (001) plane was observed. Moreover, a metastable phase was formed, $\beta\text{-V}_2\text{O}_5$, as a result of oxygen loss from $\alpha\text{-V}_2\text{O}_5$ due to a reduction process [32]. It should be also pointed out that the higher intensity of V_2O_5 peaks in

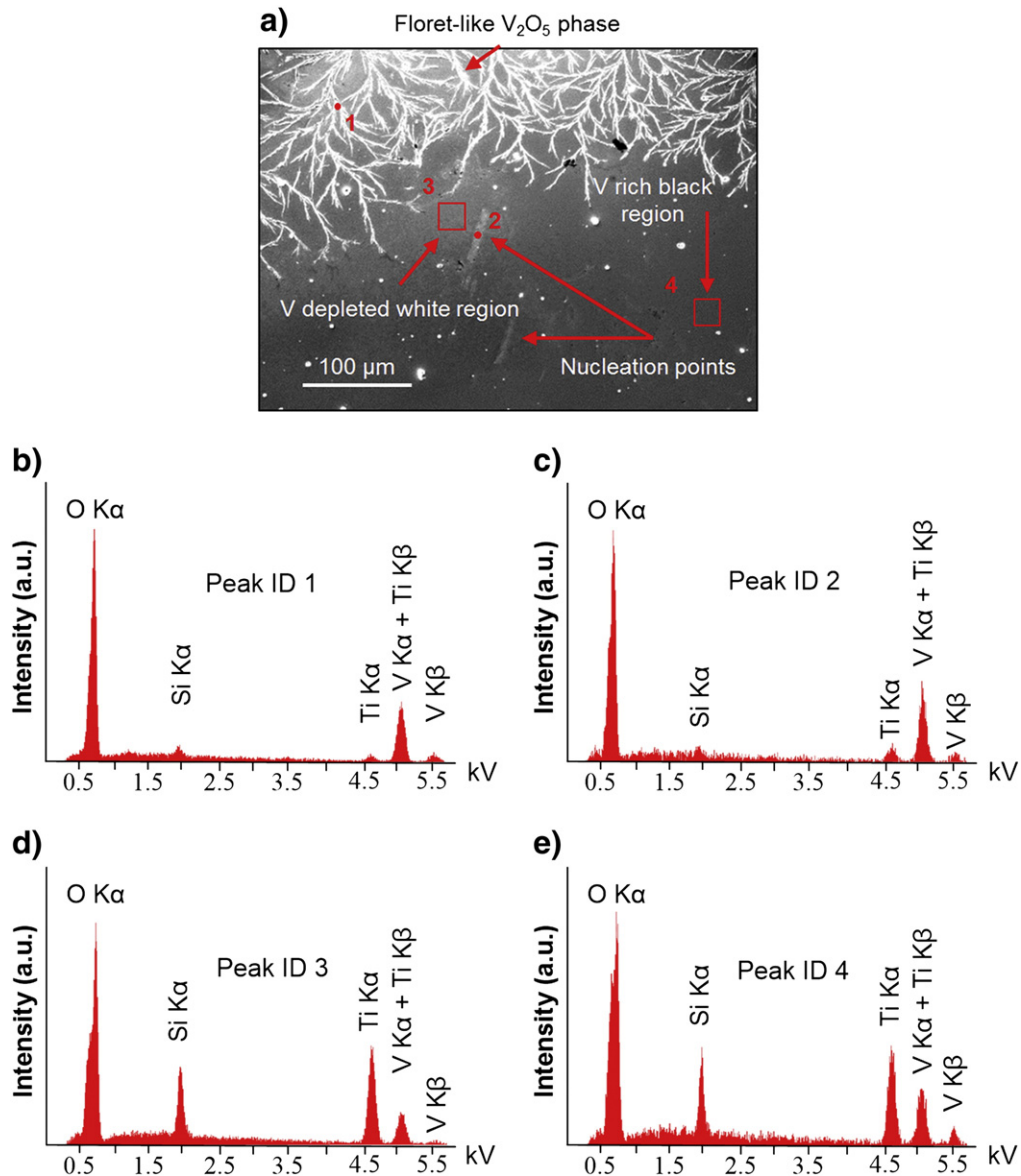


Fig. 3. a) Oxidized surface of $\text{Ti}_{0.65}\text{Si}_{0.11}\text{V}_{0.15}\text{N}$ coating isothermal tested at 550 °C during 30 min, showing the growing mechanism of V_2O_5 phase. SEM/EDS spectra of: b) point 1, c) point 2, d) zone 3, and e) zone 4.

relation to other peaks suggests higher quantity on the oxidized volume. The temperature increase to 650 °C led to suppression of TiN peaks suggesting the formation of a thick oxide scale. At 675 °C, the peaks associated with the V_2O_5 phases disappeared, which was in a good agreement with the melting point of V_2O_5 oxide [7,13,24]. On the other hand, peaks related to a V_3O_5 phase, which resulted from the α - V_2O_5 reduction, were found. In fact, in case of oxygen deficiency, a shift to lower valence state leads to the formation of reduced oxides, such as V_3O_5 identified in the current XRD pattern. Further increase in temperature resulted mostly in the increase of V_3O_5 peaks intensities due to continuous reduction of liquid V_2O_5 phase. $Ti(V)O_2$, V_3O_5 , V_2O_3 and VO reduced phases were found after annealing, as well as a new polymorph V_2O_5 oxide: γ' - V_2O_5 (ICDD card 85-2422). This oxide has an orthorhombic structure as α - V_2O_5 phase, but with different diffraction planes. These changes could be attributed to distortions on the structure motivated by the cooling of liquid-phase. Double chains exist in both phases, but VO_5 pyramids alternate up and down individually for γ' - V_2O_5 , whereas they alternate by pairs for normal α - V_2O_5 phase [33]. These results are in a good agreement with the oxide phases previously identified on the oxidized surface of the film.

The growth mechanism of the V_2O_5 phase over the $Ti(V)O_2$ oxide on the oxidized surface of the V rich film is shown in Fig. 3. SEM/EDS analyses revealed that nucleation points of V_2O_5 started being formed over the oxidized surface (see peak ID 2), growing up by vanadium lateral diffusion as suggested by the EDS spectra obtained from the V depleted white and V rich black regions marked in the SEM micrograph (zones 3 and 4, respectively). In order to investigate the oxide scale growth, TEM cross-sections were prepared by FIB from $Ti_{0.65}Si_{0.11}V_{0.15}N$ and $Ti_{0.80}Si_{0.15}N$ films annealed at 600 and 900 °C, respectively. It should be emphasized here that the different oxidation isothermal temperatures were used due to dissimilarities in the oxidation resistance of coatings as referred to above.

3.3. Cross section of oxidized surfaces by TEM and oxidation kinetics

Figs. 4 and 5 displays the bright-field STEM images, associated elemental maps and scanning elemental profiles from cross section of oxidized $Ti_{0.80}Si_{0.15}N$ and $Ti_{0.65}Si_{0.11}V_{0.15}N$ coatings. In the case of $Ti_{0.80}Si_{0.15}N$ film a multilayer of oxides can be identified, being more complex close to the film defect (white zones) shown in Fig. 4a): (i) an outer Ti-rich layer comprised by shaped crystals with bigger size in the top of the film defect, zone corresponding to the white phase and, (ii) a Si-rich layer, which is itself divided in 3 layers on the zone around the defect, an intermediate layer containing Ti, sandwiched between two Ti-free layers, being the external porous and the internal one very compact. Far from the film defect (left zone of the micrograph), below to the TiO_2 crystals only a homogeneous Si-rich layer was observed. The measured elemental cross-section depth profiles for two lines were plotted in Fig. 4b) and c), respectively. The profiles corroborated STEM/EDX elemental mapping showing in detail the composition of surface oxides. The surface layer formed exclusively of Ti–O was followed by a Si-rich layer with scattering in the signal intensity, in agreement with brightness intensity in Fig. 4a). In Ti-signal a small increase in intensity in the zone of high-Si content is clear. This variation is more intense in line 2 than in line 1, suggesting an influence of the film defect, which is closer to line 2. Continuous and compact Si–O layer at the oxide/coating interface acts as an efficient barrier against oxygen and metal ions diffusion and thus protecting the coating from further oxidation [30,31].

It is evident that Ti oxide forms first on the surface of the film due to the higher affinity of Ti for O than Si [30,31] and then, with further increase in temperature, silicon oxide is formed due to the progressive segregation of Si. The oxidation process will then occur through the inwards diffusion of O^{2-} through the TiO_2 layer and the outwards diffusion of Ti^{4+} through the Si–O layer [34]. Nevertheless, due to the

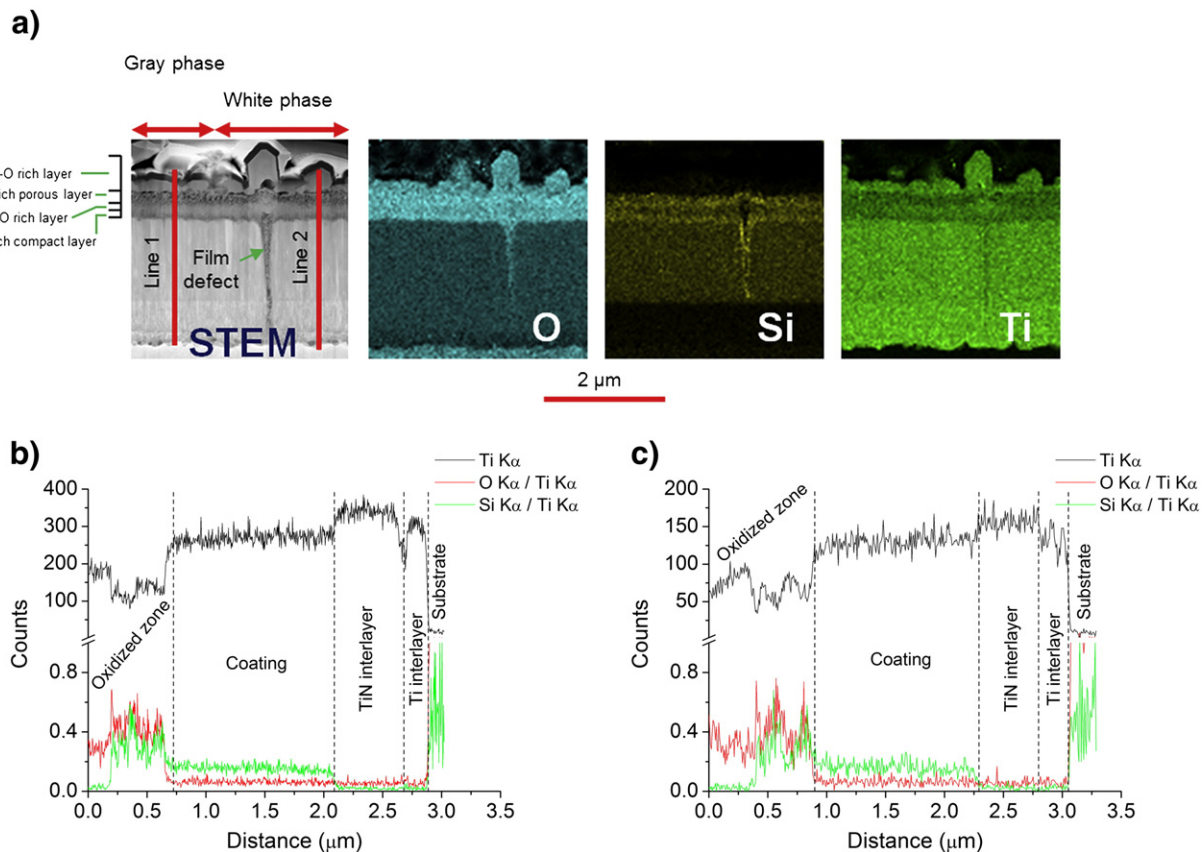


Fig. 4. a) Bright field STEM cross section and correspondent elemental maps of $Ti_{0.80}Si_{0.15}N$ coating oxidized at 900 °C during 1 h. Elemental line scans along the cross section of the oxidized coating obtained from two places: b) line 1 and c) line 2.

presence of film defects, in the first stage of the oxidation process, a high amount of Ti ions will be supplied in that zone corresponding to the oxidation occurring in the defect walls. This process will promote the formation of a porous Si–O layer, with low diffusion barrier performance to the out diffusion of Ti^{4+} ions, leading to large TiO_2 crystals on the oxide scale surface. From the moment that a Si–O barrier layer is formed in the defect walls (see Si signal in Fig. 4a)) the oxidation process will be controlled by the O^{2-} inward and Ti^{4+} outward ions diffusion through the Si–O layer [34]. It should be remarked that this phenomenon should not influence significantly the global oxidation behavior of the Ti–Si–N coating (which shows the parabolic behavior presented in Fig. 1a)), in agreement with literature [30,31,34]) since, on the one hand, it only occurs in a few defects in the film surface (see Fig. 1b)) and, on the other, it should be more intense in the first stage of the oxidation, during heating up to the 900 °C isothermal oxidation temperature.

$Ti_{0.65}Si_{0.11}V_{0.15}N$ coating exhibited, after annealing, two-layers oxide structure with a thick porous inner layer and an outer discontinuous layer of well-defined crystals. The elemental maps shown in Fig. 5a) suggested that the majority of vanadium was located in the outer crystal layer, whereas inner layer was Ti and Si rich. These results corroborate the detection of the rutile type compound $Ti(V)O_2$ and V_2O_5 indexed by XRD and Raman spectroscopy in the light and dark phases in Fig. 1c) [26], for the sub-surface and top oxide layer respectively. Further, the presence of Si–O at the sub-surface is in agreement with the EDS results shown in our previous work [26]. Elemental lines shown in Fig. 5b) and c) showed that diffusion of V occurred exclusively within the oxidized volume, since V is almost completely depleted in the inner oxide layer whereas no V gradient is detected in the non-oxidized coating, as shown by the constant V signal across this zone. In general, we observed a thicker non-oxidized layer in the regions covered by V–O crystal phase. Furthermore, comparing either the V content integrated intensities of Fig. 5a) and b) or the brightness of V signal between the right and

left part of Fig. 5a), it can be concluded that V has to be diffused from the left to the right zone of this figure. Finally, it should be remarked that there is no indication of formation of any Si-rich layer, being Si signal uniformly distributed in both oxide scale and non-oxidized coating. Therefore, a dense compact protective silicon oxide layer localized in subsurface was not formed being Si–O randomly distributed in the $Ti(V)O_2$ porous scale.

Isothermal curve of $Ti_{0.65}Si_{0.11}V_{0.15}N$ coating oxidized at temperatures below the melting point of V_2O_5 started with a linear increase in mass gain obeying after that to a parabolic law. A strong correlation can be found between the microstructure of the oxide scale and the isothermal oxidation curve of $Ti_{0.65}Si_{0.11}V_{0.15}N$ coating. High temperature XRD patterns shown in Fig. 2), revealed that the first oxide being formed is $Ti(V)O_2$. At the very beginning of the oxidation process, due to the high Ti content, a TiO_2 layer starts growing. The presence of V ions and its high solubility with Ti promote the formation of $Ti(V)O_2$ solid solution, which comprises vanadium cations with lower oxidation states as V^{3+} ions [15,35]. The substitution of Ti^{4+} by V^{3+} ions in the TiO_2 lattice would increase the concentration of interstitial metallic Ti^{4+} ions and decrease the number of excess electrons and consequently increasing the oxidation rate. This justifies the initial rapid oxidation observed in the isothermal curve, in good agreement to the work of Thongtem et al. [35] who studied the effect of V doping to Ti-based alloys. At the same time that $Ti(V)O_2$ oxide is being formed, Si ions are being supplied at the interface to form Si–O. However, due to V ions diffusion through the oxide scale to the surface, the formation of a protective and compact Si–O layer is inhibited, degrading the oxidation resistance of the coatings when compared to $Ti_{0.80}Si_{0.15}N$ film. This agrees well with the elemental maps shown in Fig. 5a), where Si–O and $Ti(V)O_2$ coexist in the inner porous layer, never showing a continuous agglomeration of Si–O necessary to protect the material from oxidation. Such observations are in accordance to literature works on diffusion processes of V rich

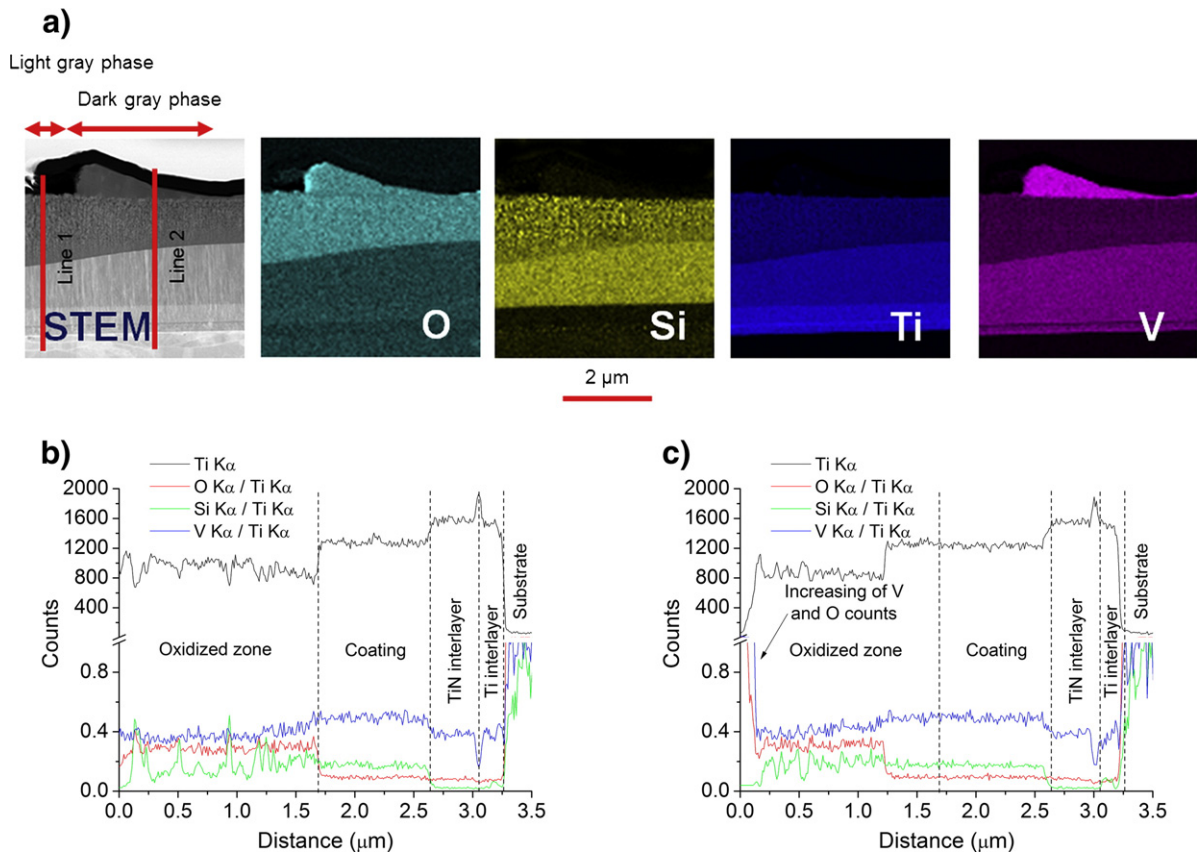


Fig. 5. a) Bright field STEM cross section and correspondent elemental maps of $Ti_{0.65}Si_{0.11}V_{0.15}N$ coating oxidized at 600 °C during 30 min. Elemental line scans along the cross section of the oxidized coating obtained from two places: b) line 1 and c) line 2.

coatings, where an inner porous layer was always formed due to V ions migration to the surface (Refs. [24,25]). From the moment that vanadium cations, with lower oxidation states, (V^{3+} or V^{4+}) arrive to the surface, they are further oxidized to V^{5+} combining with O ions and creating nucleation points for the V_2O_5 growth, which will expand and grow up by vanadium lateral diffusion, as evidenced in Fig. 3. With the ongoing oxidation, the oxide scale became thicker and the isothermal curve started to obey to a parabolic law due to a reduction of ions mobility through the oxide scale. The process develops leading to the formation of a porous rich inner Ti(V)O₂ and Si–O layer and an outer most dispersed V_2O_5 one, that can comprise both α - V_2O_5 and β - V_2O_5 phases as evidenced in the XRD patterns at high temperature.

4. Conclusion

In this investigation, the effect of V additions on the oxidation and diffusion processes occurring during Ti_{0.65}Si_{0.11}V_{0.15}N film annealing is studied and related to the behavior of ternary Ti_{0.80}Si_{0.15}N system. In summary, we demonstrated that oxidation of Ti_{0.80}Si_{0.15}N is controlled by the formation of a dense and compact silicon oxide acting as a diffusion barrier, which can be affected by defects in the as-deposited film. The presence of V cations with lower oxidation states in the TiO₂ scale, during the oxidation of Ti_{0.65}Si_{0.11}V_{0.15}N film, was responsible for a significant increase of the oxidation rate and the inability of formation of a Si–O protective oxide.

Acknowledgments

This research is sponsored by FEDER funds through the program COMPETE – Programa Operacional Factores de Competitividade – and by national funds through FCT – Fundação para a Ciência e a Tecnologia, under the projects: PTDC/EME-TME/122116/2010 and PTDC/EMS-TEC/1805/2012, as well as the grant SFRH/BD/68740/2010. T. Polcar acknowledges support from the project MSM 68407 70038.

References

- [1] C. Muratore, A.A. Voevodin, Chameleon Coatings: adaptive surfaces to reduce friction and wear in extreme environments, Annual Review of Materials Research, Annual Reviews, Palo Alto, 39 2009, pp. 297–324.
- [2] N. Fateh, G.A. Fontalvo, G. Gassner, C. Mitterer, Influence of high-temperature oxide formation on the tribological behaviour of TiN and VN coatings, Wear 262 (2007) 1152–1158.
- [3] E. Badisch, G.A. Fontalvo, M. Stoiber, C. Mitterer, Tribological behavior of PACVD TiN coatings in the temperature range up to 500 °C, Surf. Coat. Technol. 163–164 (2003) 585–590.
- [4] M. Stoiber, E. Badisch, C. Lugmair, C. Mitterer, Low-friction TiN coatings deposited by PACVD, Surf. Coat. Technol. 163–164 (2003) 451–456.
- [5] T. Polcar, A. Nossa, M. Evaristo, A. Cavaleiro, Nanocomposite coatings of carbon-based and transition metal dichalcogenides phases: a review, Rev. Adv. Mater. Sci. 15 (2007) 118–126.
- [6] S.M. Aouadi, H. Gao, A. Martini, T.W. Scharf, C. Muratore, Lubricious oxide coatings for extreme temperature applications: a review, Surf. Coat. Technol. 257 (2014) 266–277.
- [7] R. Franz, C. Mitterer, Vanadium containing self-adaptive low-friction hard coatings for high-temperature applications: a review, Surf. Coat. Technol. 228 (2013) 1–13.
- [8] T.W. Scharf, S.V. Prasad, Solid lubricants: a review, J. Mater. Sci. 48 (2013) 511–531.
- [9] A.A. Voevodin, C. Muratore, S.M. Aouadi, Hard coatings with high temperature adaptive lubrication and contact thermal management: review, Surf. Coat. Technol. 257 (2014) 247–265.
- [10] D.B. Lewis, S. Creasey, Z. Zhou, J.J. Forsyth, A.P. Ehiassarian, P.E. Hovsepian, Q. Luo, W.M. Rainforth, W.D. Münz, The effect of (Ti + Al): V ratio on the structure and oxidation behaviour of TiAlN/VN nano-scale multilayer coatings, Surf. Coat. Technol. 177–178 (2004) 252–259.
- [11] K. Kutschej, P.H. Mayrhofer, M. Kathrein, P. Polcik, C. Mitterer, A new low-friction concept for Ti_{1-x}Al_xN based coatings in high-temperature applications, Surf. Coat. Technol. 188–189 (2004) 358–363.
- [12] K. Kutschej, P.H. Mayrhofer, M. Kathrein, P. Polcik, C. Mitterer, Influence of oxide phase formation on the tribological behaviour of Ti–Al–V–N coatings, Surf. Coat. Technol. 200 (2005) 1731–1737.
- [13] G. Gassner, P.H. Mayrhofer, K. Kutschej, C. Mitterer, M. Kathrein, A new low friction concept for high temperatures: lubricious oxide formation on sputtered VN coatings, Tribol. Lett. 17 (2004) 751–756.
- [14] P.H. Mayrhofer, P.E. Hovsepian, C. Mitterer, W.D. Münz, Calorimetric evidence for frictional self-adaptation of TiAlN/VN superlattice coatings, Surf. Coat. Technol. 177–178 (2004) 341–347.
- [15] A. Glaser, S. Surnev, F.P. Netzer, N. Fateh, G.A. Fontalvo, C. Mitterer, Oxidation of vanadium nitride and titanium nitride coatings, Surf. Sci. 601 (2007) 1153–1159.
- [16] M. Uchida, N. Nihira, A. Mitsuo, K. Toyoda, K. Kubota, T. Aizawa, Friction and wear properties of CrAlN and CrVN films deposited by cathodic arc ion plating method, Surf. Coat. Technol. 177–178 (2004) 627–630.
- [17] J.H. Ouyang, S. Sasaki, Tribo-oxidation of cathodic arc ion-plated (V, Ti)N coatings sliding against a steel ball under both unlubricated and boundary-lubricated conditions, Surf. Coat. Technol. 187 (2004) 343–357.
- [18] J.-K. Park, Y.-J. Baik, Increase of hardness and oxidation resistance of VN coating by nanoscale multilayered structuration with AlN, Mater. Lett. 62 (2008) 2528–2530.
- [19] R. Franz, J. Neidhardt, R. Kaindl, B. Sartory, R. Tessadri, M. Lechthaler, P. Polcik, C. Mitterer, Influence of phase transition on the tribological performance of arc-evaporated AlCrVN hard coatings, Surf. Coat. Technol. 203 (2009) 1101–1105.
- [20] Y. Qiu, S. Zhang, J.-W. Lee, B. Li, Y. Wang, D. Zhao, Self-lubricating CrAlN/VN multilayer coatings at room temperature, Appl. Surf. Sci. 279 (2013) 189–196.
- [21] M. Pfeiler, K. Kutschej, M. Penoy, C. Michotte, C. Mitterer, M. Kathrein, The effect of increasing V content on structure, mechanical and tribological properties of arc evaporated Ti–Al–V–N coatings, Int. J. Refract. Met. Hard Mater. 27 (2009) 502–506.
- [22] W. Tillmann, S. Momeni, F. Hoffmann, A study of mechanical and tribological properties of self-lubricating TiAlVN coatings at elevated temperatures, Tribol. Int. 66 (2013) 324–329.
- [23] Q. Luo, Temperature dependent friction and wear of magnetron sputtered coating TiAlN/VN, Wear 271 (2011) 2058–2066.
- [24] Z. Zhou, W.M. Rainforth, C. Rodenburg, N.C. Hyatt, D.B. Lewis, P.E. Hovsepian, Oxidation behavior and mechanisms of TiAlN/VN coatings, Metall. Mater. Trans. A 38 (2007) 2464–2478.
- [25] R. Franz, J. Neidhardt, C. Mitterer, B. Schaffer, H. Hutter, R. Kaindl, B. Sartory, R. Tessadri, M. Lechthaler, P. Polcik, Oxidation and diffusion processes during annealing of AlCrVN hard coatings, J. Vac. Sci. Technol. A 26 (2008) 302–308.
- [26] F. Fernandes, A. Loureiro, T. Polcar, A. Cavaleiro, The effect of increasing V content on the structure, mechanical properties and oxidation resistance of Ti–Si–V–N films deposited by DC reactive magnetron sputtering, Appl. Surf. Sci. 289 (2014) 114–123.
- [27] F. Fernandes, T. Polcar, A. Cavaleiro, Tribological properties of self-lubricating TiSiVN coatings at room temperature, Surf. Coat. Technol. 267 (2015) 8–14.
- [28] D.P. Alexander, P.S. Anatolii, A.A. Nikolai, M.B. Vyacheslav, Structures and properties of hard and superhard nanocomposite coatings, Physics-Uspekhi 52 (2009) 29.
- [29] A. Mège-Revil, P. Steyer, S. Cardinal, G. Thollet, C. Esnouf, P. Jacquot, B. Stauffer, Correlation between thermal fatigue and thermomechanical properties during the oxidation of multilayered TiSiN nanocomposite coatings synthesized by a hybrid physical/chemical vapour deposition process, Thin Solid Films 518 (2010) 5932–5937.
- [30] T. Kacsich, S. Gasser, Y. Tsuji, A. Dommann, M.A. Nicolet, A. Nicolet, Wet oxidation of Ti₃₄Si₂₃B₄₃, J. Appl. Phys. 85 (1999) 1871–1875.
- [31] T. Kacsich, M.A. Nicolet, Moving species in Ti₃₄Si₂₃N₄₃ oxidation, Thin Solid Films 349 (1999) 1–3.
- [32] A. Bouzidi, N. Benramdane, S. Bresson, C. Mathieu, R. Desfeux, M.E. Marssi, X-ray and Raman study of spray pyrolysed vanadium oxide thin films, Vib. Spectrosc. 57 (2011) 182–186.
- [33] J.M. Cocciantelli, P. Gravereau, J.P. Doumerc, M. Pouchard, P. Hagenmuller, On the preparation and characterization of a new polymorph of V₂O₅, J. Solid State Chem. 93 (1991) 497–502.
- [34] F. Deschoux-Beaume, N. Frety, T. Cutard, C. Colin, Oxidation modeling of a Si₃N₄–TiN composite: comparison between experiment and kinetic models, Ceram. Int. 35 (2009) 1709–1718.
- [35] S. Thongtem, T. Thongtem, M. McNallan, High-temperature nitridation and oxidation of Ti-based alloys, Surf. Interface Anal. 32 (2001) 306–309.